DOI: 10.1002/ejic.200600673

Dimeric Complexes of Lanthanide(III) Hexafluoroacetylacetonates with 4-Cyanopyridine *N*-Oxide: Synthesis, Crystal Structure, Magnetic and Photoluminescent Properties

Svetlana V. Eliseeva,*[a] Mikhail Ryazanov,*[a,b] Frédéric Gumy,[c] Sergey I. Troyanov,[a] Leonid S. Lepnev,[d] Jean-Claude G. Bünzli,[c] and Natalia P. Kuzmina[a]

Keywords: Lanthanides / β-Diketonates / Luminescence / Thin films / Photophysics

A series of new mixed-ligand lanthanide complexes $[Ln(hfa)_3(4\text{-cpyNO})]_2$ ($Ln = Sm^{III}$–Ho^{III} and Tm^{III}; hfa^- = hexafluoroacetylacetonate; 4-cpyNO = 4-cyanopyridine *N*-oxide) have been synthesised by treating the corresponding lanthanide hexafluoroacetylacetonates with 4-cpyNO (molar ratio 1:1) in chloroform. Single-crystal X-ray analysis revealed that $[Tb(hfa)_3(4\text{-cpyNO})]_2$ and $[Ho(hfa)_3(4\text{-cpyNO})]_2$ are isostructural and are comprised of two types of symmetrically independent dimetallic molecules. Within a dimer, the eight-fold-coordinated metal atoms are bridged by two 4-cpyNO ligands through the oxygen atoms of the *N*-oxide groups. The magnetic susceptibility data for the Gd^{III} and Tb^{III} complexes indicate the presence of weak antiferromagnetic interactions within the dimetallic Ln_2O_2 units. The thermal stability of the $[Ln(hfa)_3(4\text{-cpyNO})]_2$ adducts was studied by thermogravimetric analysis and their volatility estimated from sublimation experiments under reduced pressure. The photoluminescent properties were measured for solid samples upon excitation at 330–360 nm. The mixed-ligand complexes of Sm^{III}, Eu^{III}, Tb^{III}, Dy^{III} and Tm^{III} exhibit metal-centred luminescence in the entire visible spectral range with characteristic pink, red, green, yellow and blue emission, respectively. The introduction of ancillary 4-cpyNO molecules into the coordination sphere of the lanthanide(III) ions was found to significantly affect their luminescence quantum yields. $[Eu(hfa)_3(4\text{-cpyNO})]_2$ thin films on quartz substrates were obtained by the vacuum evaporation technique and their photoluminescent properties were found to be enhanced when compared with those of the bulk samples. This suggests that these dimers could be good candidates for the fabrication of emitting layers for light-emitting diodes.

Introduction

Luminescent lanthanide complexes with organic ligands are of great interest since they can be used, for instance, as light-converting optical materials, light-emitting layers in electroluminescent (EL) devices,[1] contrast agents for magnetic resonance imaging[2] and luminescent probes in biology.[3] Such coordination compounds are chemically stable and provide a versatile tool for tuning their spectroscopic properties both by choosing the appropriate lanthanide ions as well as by changing the characteristics of the organic ligands, such as by introducing suitable substituents/atoms or conjugated π-electron fragments.[4,5]

The aim of this work is to develop and test highly luminescent lanthanide(III) complexes that can be utilized for fabricating light-emitting thin films. Lanthanide tris(β-diketonate) chelates are among the most investigated Ln^{III} coordination compounds as they exhibit sharp emission bands in the visible and near-infrared spectral ranges. These compounds usually crystallise with solvent molecules, which are detrimental to their photophysical properties. To overcome the solvent-quenching problem, an additional β-diketonate ligand can be introduced to give anionic lanthanide(III) complexes, or, alternatively, neutral chromophoric ligands may be used as ancillary ligands to saturate the inner coordination sphere of the metal ion. In the latter case, the sensitisation of lanthanide luminescence can be additionally improved when the ancillary ligand possesses suitable energy levels to provide an effective intramolecular energy transfer from the ligand to the lanthanide ion.[5] For further

[a] Lomonosov Moscow State University, Department of Chemistry,
Leninskie Gory, 119992 Moscow, Russia
Fax: +7-495-939-0998
E-mail: eliseeva@inorg.chem.msu.ru
[b] Max-Planck Institut für Festkörperforschung
Heisenbergstr. 1, 70569 Stuttgart, Germany
Fax: +49-711-689-1091
E-mail: m.ryazanov@fkf.mpg.de
[c] École Polytechnique Fédérale de Lausanne (EPFL), Laboratory of Lanthanide Supramolecular Chemistry,
BCH 1405, 1015 Lausanne, Switzerland
Fax: +41-21-693-9825
E-mail: jean-claude.bunzli@epfl.ch
[d] Lebedev Physical Institute of Russian Academy of Sciences, Vavilov Luminescence Laboratory,
Leninsky Prospect 53, 119991 Moscow, Russia
Fax: +7-495-938-2251
E-mail: lepn@sci.lebedev.ru

Supporting information for this article is available on the WWW under http://www.eurjic.org or from the author.

potential application of luminescent complexes as emitting layers, for example in organic light-emitting diodes, it is interesting and useful to investigate their photoluminescent properties in thin films. It is well known that the luminescence of lanthanide(III) ions, especially Eu^{III}, is very sensitive to the local micro-environment of the ion.[6] As a consequence, the packing of the molecules in the crystal structure, the sample form (solid/powder, thin film or solution) and even the deposition method of thin films (vacuum evaporation, spin-coating, etc.) may have a significant influence on the luminescence lifetimes and quantum yields. However, only a few studies have been devoted to this question.[7]

In this paper, we report the synthesis, structural study and thermal analysis of the new mixed-ligand lanthanide(III) complexes $[Ln(hfa)_3(4\text{-cpyNO})]_2$ (Ln = Sm^{III}–Ho^{III}, Tm^{III}) with 4-cyanopyridine *N*-oxide as a bridging ligand to link the metal atoms into dimetallic molecular species. The luminescent and magnetic properties of these compounds were studied and the effect of introducing the ancillary 4-cpyNO ligands on their luminescence characteristics is discussed. Furthermore, in order to assess the potential of the dimeric complexes for light-emitting layers in electroluminescent devices, thin films of $[Eu(hfa)_3(4\text{-cpyNO})]_2$ were obtained by the vacuum evaporation technique and their photoluminescent properties compared with those of the bulk samples.

Results and Discussion

Synthesis and Characterisation

The reaction of 4-cyanopyridine *N*-oxide with an equimolar amount of $[Ln(hfa)_3(H_2O)_2]$ in chloroform yields air-stable complexes $[Ln(hfa)_3(4\text{-cpyNO})]_2$ (Ln = Sm^{III}–Ho^{III}, and Tm^{III}), which were isolated as colourless (Gd^{III}, Tb^{III}), pale yellow (Sm^{III}, Eu^{III}, Ho^{III} and Dy^{III}) or pale aquamarine (Tm^{III}) polycrystalline precipitates by removing part of the solvent at low pressure. The formation of the mixed-ligand lanthanide adducts was confirmed by elemental analysis and IR spectroscopy. The IR spectra of all the complexes obtained are similar, exhibiting C=O and C=C absorption bands in the region 1700–1500 cm^{-1} that are typical of lanthanide chelate complexes containing fluorinated β-diketonate ligands.[8] The characteristic bands due to the terminal C≡N group and pyridine *N*-oxide C–H vibrations of the 4-cpyNO ligand appear in the ranges 2300–2200 cm^{-1} and 3200–3000/900–600 cm^{-1}, respectively. The

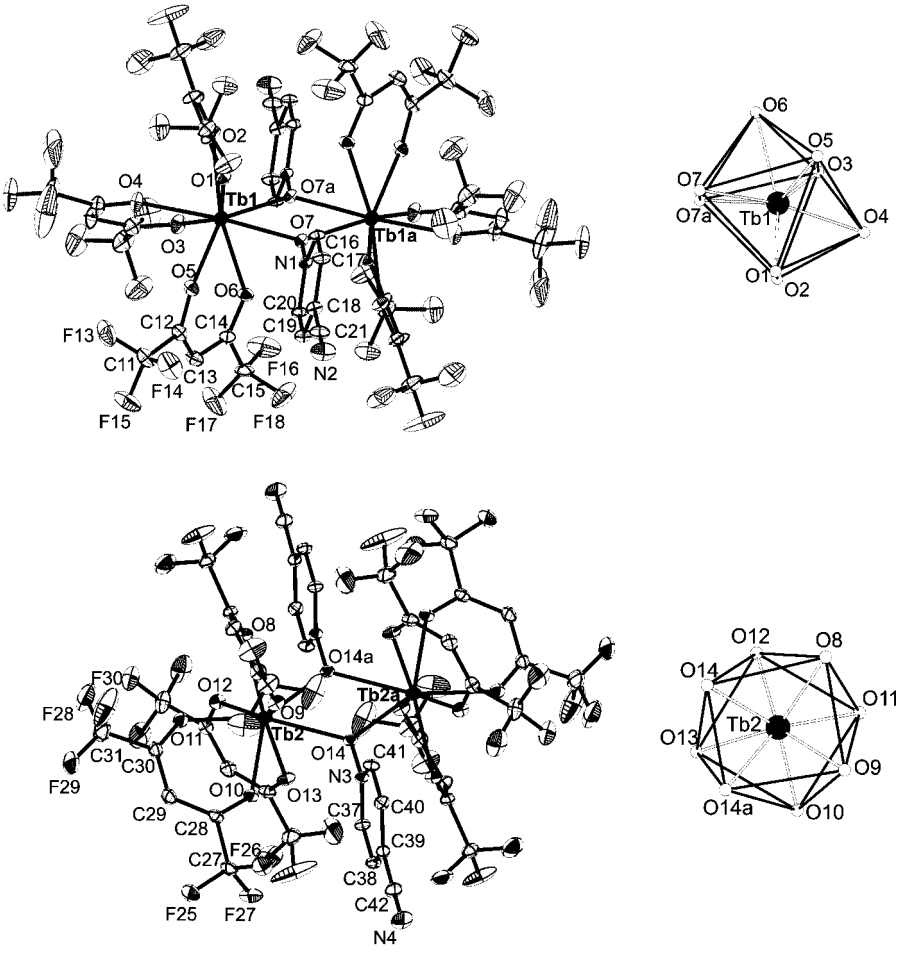

Figure 1. Molecular structures of the centrosymmetric LnL-1 and LnL-2 species in the crystal structure of $[Tb(hfa)_3(4\text{-cpyNO})]_2$ with coordination polyhedra around the metal atoms outlined (30% probability level ellipsoids). Hydrogen atoms omitted for clarity.

assignment of the bands at 1300–1100 cm^{-1} is difficult due to overlap of the ν(N–O) and ν(C–F) vibrations. The absence of absorption between 3600 and 3200 cm^{-1} implies that these compounds contain no water molecules.

Crystal and Molecular Structures

Single crystals of $[Tb(hfa)_3(4\text{-cpyNO})]_2$ and $[Ho(hfa)_3(4\text{-cpyNO})]_2$ were obtained from chloroform, and their structures were determined by X-ray crystallography (see Experimental Section for further details). Both compounds are isostructural, crystallising in the monoclinic space group $P2_1/c$ with $Z = 4$. The crystal structure consists of two types of symmetrically independent centrosymmetric dimetallic $[Ln(hfa)_3(4\text{-cpyNO})]_2$ molecules, hereafter referred to as LnL-1 and LnL-2, which differ from each other mainly in the coordination geometry of the lanthanide atoms (vide infra). Perspective views of the molecules, with the LnO_8 polyhedra outlined, are given in Figure 1 for the Tb^{III} derivative. Selected bond lengths and angles are summarised in Table 1. Within a dimer, the metal ions are eight-coordinated by oxygen atoms from two bridging μ-4-cpyNO ligands and from three hfa^- anions, which act as didentate chelating ligands. The bridging LnOOLn(a) core is completely planar due to the presence of an inversion centre. Intramolecular Ln···Ln separations across the Ln–O–Ln(a) vary in the range 3.99–4.13 Å (Table 1). A detailed analysis of the molecular geometry[9,10] reveals that the metal atoms in LnL-1 have a distorted bicapped trigonal-prismatic (BCTP) coordination environment, whereas those in LnL-2 have square-antiprismatic (SAP) coordination (cf. Table 2). In the BCTP polyhedron, the trigonal faces are formed by atoms O1, O5, O7 and O2, O3, O7a, respectively, while the O4 and O6 atoms cap two quadrilateral faces of the trigonal prism. The dihedral angle between the trigonal planes is 18.4°. In the SAP polyhedron, the square faces are delimited by atoms O10, O11, O12, O13 and O8, O9, O14, O14a, respectively, with the dihedral angle between the corresponding planes being 2.8°. The different coordination patterns observed are likely due to steric effects. The planar 4-cpyNO units in LnL-1 are arranged nearly perpendicular relative to the bridging Ln_2O_2 plane ($\phi = 86.4°$), thus minimizing the steric hindrance of the β-diketonate ligands. These units become more twisted toward the hfa^- ligands ($\phi = 80.7°$) in the LnL-2 molecules, leading to distortion of the oxygen atoms along a pathway from SAP to BCTP. It is interesting to note a structural difference between $[Tb(hfa)_3(4\text{-cpyNO})]_2$ and a related adduct of Eu^{III} hexafluoroacetylacetonate with pyridine *N*-oxide, namely $[Eu_2(hfa)_6(pyNO)_3]$:[11] the crystal structure of the latter also contains dimetallic species, although the metal atoms are nine-coordinate and are bridged by three μ-pyNO ligands.

A regular deviation in the mean values of the Ln–O(β-diketonate) bond lengths and O–Ln–O angles is found when comparing the Tb^{III} and Ho^{III} structures (2.38–2.33 Å and 72.4–73.0°, respectively), consistent with a decreasing size of the metal atom. The Ln–O distances for the neutral 4-cpyNO ligands are longer than those for the anionic hfa^- ligands, ranging from 2.416 to 2.435 Å (Tb^{III}) and from 2.372 to 2.393 Å (Ho^{III}).

The symmetrically independent LnL-1 and LnL-2 molecules in the crystal structure of $[Ln(hfa)_3(4\text{-cpyNO})]_2$ are interconnected by weak intermolecular CH···N hydrogen bonds (Table 1) and lone-pair–π interactions between the 4-cpyNO species to form two-dimensional molecular assemblies in the *ac* plane (Figure 2). In the Tb^{III} complex, the substituted pyridine *N*-oxide fragments of LnL-1 and LnL-2 are aligned almost orthogonally to each other, with the nitrile N atoms being either involved in hydrogen bonding with the CH groups of neighbouring 4-cpyNO species [C(H)···N = 3.22 Å] or directed towards the pyridine ring of the neighbours with a distance to its centre of 3.54 Å.

Table 1. Selected bond lengths [Å] and angles [°] in the crystal structures[a] of $[Tb(hfa)_3(4\text{-cpyNO})]_2$ and $[Ho(hfa)_3(4\text{-cpyNO})]_2$.

	$[Tb(hfa)_3(4\text{-cpyNO})]_2$		$[Ho(hfa)_3(4\text{-cpyNO})]_2$	
	TbL-1	TbL-2	HoL-1	HoL-2
Ln···Ln	4.065(3)	4.129(3)	3.991(5)	4.050(5)
Ln–O1(O8)	2.354(3)	2.347(3)	2.312(5)	2.304(5)
Ln–O2(O9)	2.348(3)	2.365(3)	2.306(5)	2.325(5)
Ln–O3(O10)	2.306(4)	2.332(3)	2.267(5)	2.294(5)
Ln–O4(O11)	2.352(4)	2.367(4)	2.323(6)	2.329(5)
Ln–O5(O12)	2.343(4)	2.340(4)	2.298(5)	2.301(5)
Ln–O6(O13)	2.442(3)	2.399(3)	2.418(5)	2.353(5)
Ln–O7(O14)	2.435(3)	2.433(3)	2.378(5)	2.382(5)
Ln–O7a(O14a)	2.416(3)	2.429(3)	2.372(5)	2.393(5)
N1–O7 (N3–O14)	1.357(5)	1.365(4)	1.348(7)	1.348(7)
H17···N4[b] [CH···N]	2.462(1)		2.430(1)	
C39···N2	3.248(1)		3.149(1)	
Ln–O7–Ln1a (Ln–O14–Ln1a)	113.9(1)	116.3(1)	114.3(2)	116.0(2)
O1–Ln–O2 (O8–Ln–O9)	73.6(1)	72.2(1)	74.5(2)	72.9(2)
O3–Ln–O4 (O10–Ln–O11)	73.2(1)	72.6(1)	74.0(2)	73.2(2)
O5–Ln–O6 (O12–Ln–O13)	70.9(1)	72.0(1)	71.3(2)	72.1(2)
O7–Ln–O7a (O14–Ln–O14a)	66.1(1)	63.7(1)	65.7(2)	64.0(2)
N1–O7–Ln (N3–O14–Ln)	122.0(2)	122.9(2)	122.4(4)	123.7(4)
C17–H17···N4	138.7(2)		133.7(2)	
C21–N2···C39	178.1(1)		178.8(2)	

[a] Atom labels referring to the LnL-2 molecules are displayed in round prentheses. [b] Code of symmetry operations: $1 - x$, $1 - y$, $-z$.

Table 2. Observed and ideal dihedral angles for eight-coordinate complexes.

Polyhedral complexes	Angles [°]
Ideal dodecahedron	29.5, 29.5, 29.5, 29.5
Ideal square antiprism	0, 0, 52.4, 52.4
Ideal bicapped trigonal prism	0, 21.8, 48.2, 48.2
$[Tb(hfa)_3(4\text{-cpyNO})]_2$	
TbL-1	2.4, 16.0, 43.3, 47.2
TbL-2	1.2, 6.0, 46.9, 50.6
$[Ho(hfa)_3(4\text{-cpyNO})]_2$	
HoL-1	3.1, 16.4, 42.3, 47.2
HoL-2	1.4, 4.7, 47.4, 51.0

The latter suggests interactions between nitrogen lone pairs and the π-electrons of the pyridine system. The CN groups are located substantially off the ring's centre axis so that the angle, α, between the line pointing towards the centre of the pyridine ring and its face amounts to about 66° (see Figure 2). According to ab initio studies on the interaction of water with hexafluorobenzene,[12] a similar off-axis geometry is also favourable for this system and is likely to result from optimisation of the electrostatic interactions.

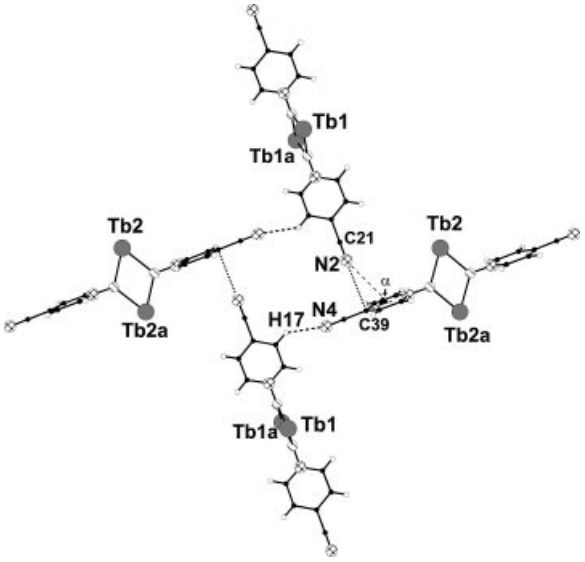

Figure 2. Packing of 4-cpyNO entities in the crystal structure of $[Tb(hfa)_3(4\text{-cpyNO})]_2$.

Magnetic Properties

The short metal–metal distances (3.99–4.13 Å) within the $[Ln(hfa)_3(4\text{-cpyNO})]_2$ complexes make these compounds interesting for a study of the magnetic exchange interactions between the paramagnetic centres. We have recently reported the magnetic properties of a related dimeric manganese(II) complex, $[Mn(hfa)_2(4\text{-cpyNO})]_2$, which exhibits weak ferromagnetic coupling at low temperatures.[13] Here, temperature-dependent studies of the magnetic susceptibility (χ_m) are presented for the gadolinium(III) and terbium(III) complexes. The former compound was found to be isostructural with the Tb^{III} derivative, as evidenced by X-ray powder diffraction experiments.

The temperature dependence of the $\chi_m T$ product for $[Gd(hfa)_3(4\text{-cpyNO})]_2$ combined with a plot of χ_m^{-1} vs. T is shown in Figure 3. At room temperature, the $\chi_m T$ value is about 15.7 $cm^3 mol^{-1} K$, close to that expected for two non-interacting Gd^{III} ions (15.75 $cm^3 mol^{-1} K$). Upon cooling, it remains almost constant until 70 K. At lower temperatures, $\chi_m T$ passes through a small maximum at 40 K before decreasing to a value of 14.96 $cm^3 mol^{-1} K$ at 2 K. This characteristic drop in $\chi_m T$ is indicative of weak antiferromagnetic Gd^{III}–Gd^{III} interactions within the dimeric molecules. A quantitative analysis of the magnetic data has been carried out using Equation (1) derived from the isotropic spin Hamiltonian $H = -JS_{Gd1} \cdot S_{Gd2}$, where J is the exchange coupling parameter and S_{Gd1} and S_{Gd2} are the spin operators associated with the interacting spin centres ($S_{Gd1} = S_{Gd2} = 7/2$).

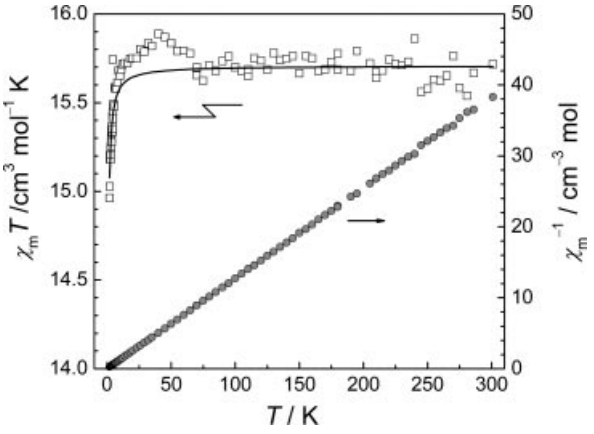

Figure 3. Temperature dependence of $\chi_m T$ (open squares) and χ_m^{-1} (filled circles) for $[Gd(hfa)_3(4\text{-cpyNO})]_2$; the solid line represents the best-fit calculated values.

$$\chi_m T = \frac{2Ng^2\mu_B^2}{k} \frac{140+91e^{7x}+55e^{13x}+30e^{18x}+14e^{22x}+5e^{25x}+e^{27x}}{15+13e^{7x}+11e^{13x}+9e^{18x}+7e^{22x}+5e^{25x}+3e^{27x}+e^{28x}}, x = -J/kT \quad (1)$$

Least-squares fitting of the experimental data with Equation (1) leads to the following parameters: J = –0.010(1) cm^{-1} and g = 1.99. The good agreement between the observed and calculated values is reflected by a small value of the R factor ($R = 2.7 \times 10^{-5}$), defined as $\Sigma[(\chi_m T)_{calc} - (\chi_m T)_{obs}]^2/\Sigma[(\chi_m T)_{obs}]^2$. The weak antiferromagnetic coupling between the Gd^{III} ions in $[Gd(hfa)_3(4\text{-cpyNO})]_2$ is further evidenced by the $\chi_m^{-1}(T)$ data, which obey a Curie–Weiss law in the whole temperature range studied (Figure 3), thereby yielding an effective magnetic moment, μ_{eff}, of 15.80(1) μ_B (per formula unit) and a negative Curie–Weiss temperature, θ, of –0.3(1) K.

For $[Tb(hfa)_3(4\text{-cpyNO})]_2$, the room-temperature $\chi_m T$ value of 23.3 $cm^3 mol^{-1} K$ remains almost unchanged in the 70–300 K region, and compares very well with the expected value for two magnetically isolated Tb^{III} ions (23.6 $cm^3 mol^{-1} K$). Upon decreasing the temperature below about 70 K, the $\chi_m T$ vs. T curve begins to decrease abruptly, and exhibits a change in slope at 40 K. The dramatic drop of $\chi_m T$ from 23.3 to 11.54 $cm^3 mol^{-1} K$ at 2 K is mainly due to the crystal-field splitting of the Tb^{III} ground state because of strong spin-orbit coupling, and could be indicative of a weak intramolecular antiferromagnetic coupling between the metal ions at low temperatures. The high-temperature data ($T > 100$ K) can be fitted to the Curie–Weiss law to yield an effective magnetic moment and a negative Curie–Weiss parameter of 19.3 μ_B per formula unit and –2(1) K, respectively.

Thermal Analyses and Vacuum Sublimation

The thermogravimetric analysis of $[Ln(hfa)_3(4\text{-cpyNO})]_2$ revealed a similar thermal behaviour for all the compounds studied. Figure 4 illustrates the weight loss for the Gd^{III} derivative. A single-step weight loss occurs in the range 190–280 °C, indicating that the lanthanide hexafluoroacetylacetonate adducts with 4-cyanopyridine *N*-oxide are thermally stable up to 190 °C. The total weight loss (ca. 92%) is much higher than that calculated for thermal decomposition of the complex into non-volatile gadolinium(III) oxyfluoride (ca. 79%) or Gd_2O_3 (ca. 80%), thus indicating partial sublimation of the sample under atmospheric pressure.

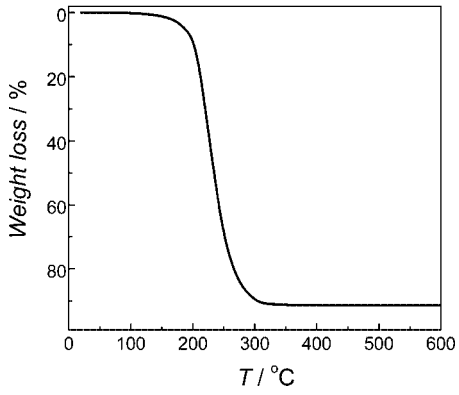

Figure 4. Thermogravimetric analysis under nitrogen for $[Gd(hfa)_3(4\text{-cpyNO})]_2$.

The vacuum sublimation experiments conducted at low pressure (10^{-2} Torr) showed that all samples are quantitatively sublimed intact at 200–220 °C according to the elemental analysis and mass spectrometric studies.[14] This allowed us to obtain good-quality thin films of the $[Eu(hfa)_3(4\text{-cpyNO})]_2$ dimer (thickness 414 ± 1 nm) by vacuum evaporation at a pressure of 10^{-6} Torr.

Photophysical Properties

The luminescence of lanthanide complexes upon excitation into the ligand absorption band arises from f–f transitions from the radiative level of Ln^{III} to their lower-lying states. It should be emphasised that transitions between the f-states are formally parity-forbidden (Laporte's rule), which, in turn, results in long radiative lifetimes (up to the millisecond timescale) and line-like emission bands.[15,16] The excited levels of Ln^{III} ions are usually populated as a result of energy transfer from the triplet level of the organic ligand, which is formed by rapid intersystem crossing. The excited level of the lanthanide(III) ion is further deactivated either radiatively with emission of light or non-radiatively by energy degradation to the vibrations of surrounding molecular groups. So, the intensity of lanthanide luminescence is determined by the ratio of the rates of radiative and non-radiative processes at all stages of the energy transfer.[17] While the emission colour and the shape of luminescence spectrum mainly depend on the electronic nature of the lanthanide ion, the energy of the triplet states of coordinated ligands plays an important role in the efficiency of the energy transfer: they should lie close to the resonant levels of the lanthanide ion but sufficiently high to prevent back energy-transfer.[18] Quenching mechanisms induced by the presence of solvent molecules in the first coordination sphere or by ligand-to-metal charge transfer (LMCT) states can also strongly influence the lanthanide luminescence.[17,19] Thus, in order to investigate the energy matching between the triplet state of the ligand and the luminescent level of the corresponding lanthanide ion, we recorded the phosphorescence spectra of solid samples of $[Gd(NO_3)_3(4\text{-cpyNO})]$, $[Gd(hfa)_3(H_2O)_2]$ and the mixed-ligand complex $[Gd(hfa)_3(4\text{-cpyNO})]_2$ at 77 K. The phosphorescence spectra of $[Gd(hfa)_3(H_2O)_2]$ and $[Gd(NO_3)_3(4\text{-cpyNO})]$ present broad bands with maxima at around 468 (21370) and 525 nm (19048 cm^{-1}), respectively (Figure 5). A small feature at 480 nm (20830 cm^{-1}) is also observed for the latter compound. The energies of zero-phonon transition of the triplet $^3\pi\pi^*$ states of the hexafluoroacetylacetonate and 4-cyanopyridine *N*-oxide ligands were thus estimated to be at around 21930 (456) and 20830 cm^{-1} (480 nm), respectively. The phosphorescence spectrum of $[Gd(hfa)_3(4\text{-cpyNO})]_2$ exhibits a broad band characterised by two maxima of almost equal intensity at about 460 (21740) and 485 nm (20620 cm^{-1}), with a shoulder at about 515 nm (19420 cm^{-1}), i.e., it resembles the superposition of the phosphorescence spectra of the organic ligands (Figure 5). Therefore, in the mixed-ligand dimetallic complexes $[Ln(hfa)_3(4\text{-cpyNO})]_2$, the energy transfer originates from both hfa^- and 4-cpyNO ligands. Figure 6 displays the energy diagram of the ligand triplet states and selected electronic levels of the lanthanide ions; the corresponding calculated energy gaps are listed in Table 3. According to empirical rules proposed for an optimal ligand-to-metal energy transfer $-2500 < \Delta E(^3\pi\pi^* - {}^5D_0) < 3500$ cm^{-1} for Eu^{III}

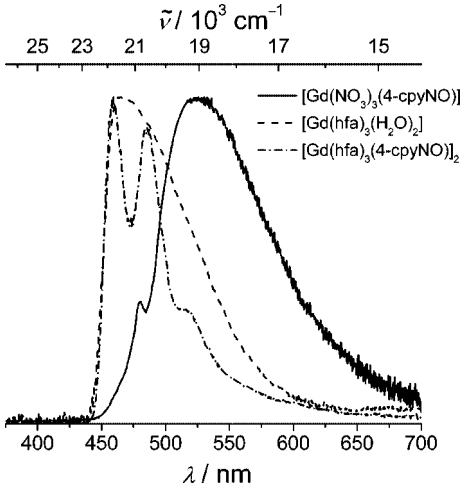

Figure 5. Phosphorescence spectra of $[Gd(NO_3)_3(4\text{-cpyNO})]$, $[Gd(hfa)_3(H_2O)_2]$ and $[Gd(hfa)_3(4\text{-cpyNO})]_2$ under excitation at 337 nm; T = 77 K.

Table 3. Energy gaps [cm^{-1}] between the triplet states of hexafluoroacetylacetonate ($^3\pi\pi^*_{hfa}$) or 4-cyanopyridine *N*-oxide ($^3\pi\pi^*_{4\text{-cpyNO}}$) and the $^4G_{5/2}$(Sm), $^5D_0$(Eu), $^5D_4$(Tb), $^4F_{9/2}$(Dy), $^1G_4$(Tm) luminescent levels of lanthanide(III) ions.

Triplet state	$\Delta E(^3\pi\pi^*–^4G_{5/2})$	$\Delta E(^3\pi\pi^*–^5D_0)$	$\Delta E(^3\pi\pi^*–^5D_4)$	$\Delta E(^3\pi\pi^*–^4F_{9/2})$	$\Delta E(^3\pi\pi^*–^1G_4)$
$^3\pi\pi^*_{hfa}$	4030	4630	1430	930	530
$^3\pi\pi^*_{4\text{-cpyNO}}$	2930	3530	330	–170	–570

ions and $2500 < \Delta E(^3\pi\pi^* - {}^5D_4) < 4000\ cm^{-1}$ for Tb^{III} ions[20] – both the hfa^- and 4-cpyNO ligands are best suited for the sensitisation of europium(III) and possibly samarium(III) luminescence. For the other Ln ions under investigation, the triplet states of the organic ligands are very close in energy to the lanthanide luminescent levels or even below, thus increasing the probability of back energy-transfer processes.

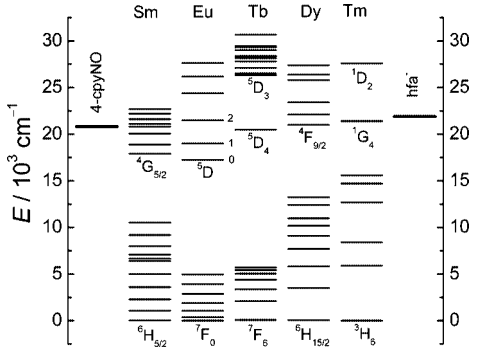

Figure 6. Energy diagram of the triplet states of the organic ligands and some energy levels of the lanthanide ions. The main luminescent and fundamental levels of the Ln ions are labelled.

To determine the influence of the substitution of water molecules by 4-cyanopyridine *N*-oxide on the photophysical properties, we compared the characteristics of solid samples of the parent $[Ln(hfa)_3(H_2O)_2]$ complexes with those of the mixed-ligand adducts $[Ln(hfa)_3(4\text{-cpyNO})]_2$.

The excitation spectra of $[Tb(hfa)_3(H_2O)_2]$ and $[Tb(hfa)_3(4\text{-cpyNO})]_2$ are very similar in shape (Figure 7) and exhibit broad bands up to 460 nm (21740 cm^{-1}), with two maxima at around 270 (37040) and 350 nm (28570 cm^{-1}) and two shoulders at 400 (25000) and 435 nm (22989 cm^{-1}), respectively. The excitation spectra of the europium(III) complexes are quite different from those of the terbium(III) derivatives and from each other (Figure 7). The excitation spectrum of $[Eu(hfa)_3(H_2O)_2]$ features a broad band ranging up to 400 nm (25000 cm^{-1}) with a maximum at around 300 nm (33333 cm^{-1}) and two weak shoulders at 330 (30303) and 360 nm (27778 cm^{-1}). In the excitation spectrum of $[Eu(hfa)_3(4\text{-cpyNO})]_2$, the intensity of the shoulders at 330 and 360 nm is larger, and they merge into a broad band extending up to 440 nm (22727 cm^{-1}) with a maximum at 275 nm (36363 cm^{-1}). Moreover, all of the excitation spectra display the characteristic bands of the metal-centred transitions at 377 and 486 nm for Tb^{III}, assigned to $^5D_3 \leftarrow {}^7F_6$ and $^5D_4 \leftarrow {}^7F_6$ transitions, and at 464 and 534 nm for Eu^{III}, corresponding to $^5D_2 \leftarrow {}^7F_0$ and $^5D_1 \leftarrow {}^7F_0$ transitions, respectively. However, the intensities of the f–f transitions are much weaker than the excitation bands of the organic ligands, thus indicating a good sensitisation of the metal-centred luminescence in these complexes through the ligand levels. As a result, under ligand excitation the Tb^{III} and Eu^{III} complexes $[Ln(hfa)_3(H_2O)_2]$ and $[Ln(hfa)_3(4\text{-cpyNO})]_2$ show bright green and red luminescence due to the $^5D_4 \rightarrow {}^7F_J$ (J = 6–0) and $^5D_0 \rightarrow {}^7F_J$ (J = 0–4) transitions,

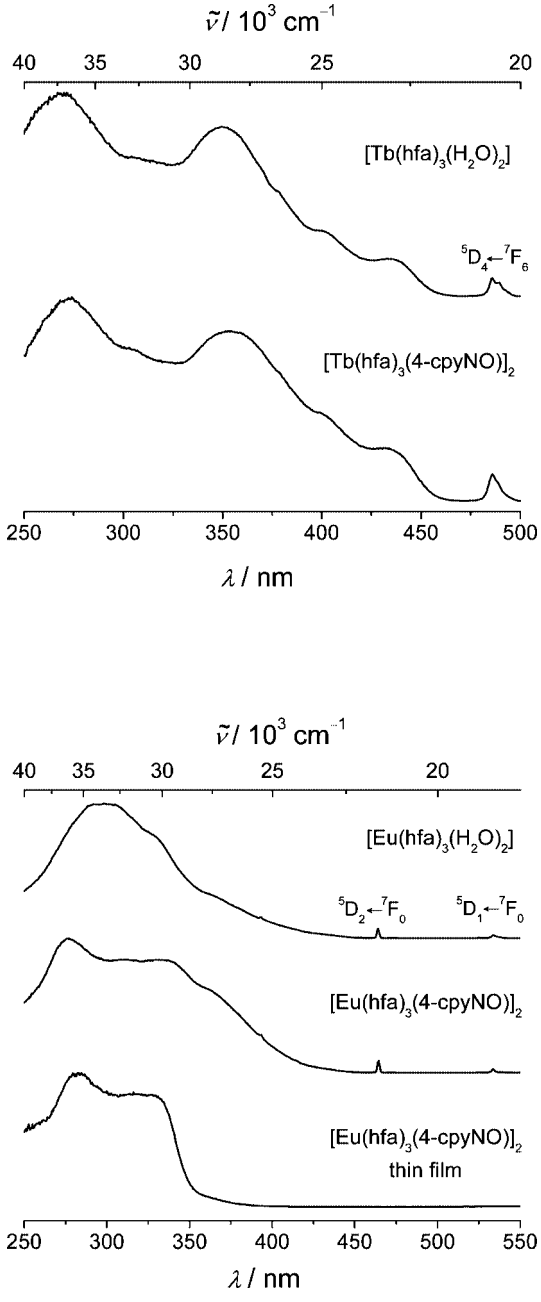

Figure 7. Excitation spectra of $[Ln(hfa)_3(H_2O)_2]$ and mixed-ligand $[Ln(hfa)_3(4\text{-cpyNO})]_2$ complexes (Ln = Eu^{III}, Tb^{III}) at 295 K.

respectively (Figure 8). No broad-band emission is observed from the triplet states of the organic ligands, thus reflecting an efficient ligand-to-metal energy transfer. The integral intensities of the $^5D_0 \rightarrow {}^7F_J$ (J = 0–4, Eu^{III}) and $^5D_4 \rightarrow {}^7F_J$ (J = 6–0, Tb^{III}) transitions are compared in Table 4. The emission spectra and relative integral intensities of the Tb^{III} complexes are essentially identical, in agreement with the fact that the terbium(III) emission bands are less sensitive to changes in the first coordination sphere of the metal centre than those of europium(III). For the Eu^{III} derivatives, the intensity of the hypersensitive $^5D_0 \rightarrow {}^7F_{2,4}$ transitions is larger for $[Eu(hfa)_3(4\text{-cpyNO})]_2$ than for $[Eu(hfa)_3(H_2O)_2]$ (Figure 8), and this is also true for the other transitions, thus implying that the introduction of the ancillary ligand increases the nephelauxetic effect. Further, the emission spectra of both complexes show only one peak for the $^5D_0 \rightarrow {}^7F_0$ transition, which points to approximately the same chemical environment around the europium(III) ions. The substitution of water molecules by 4-cyanopyridine *N*-oxide leads to an approximately threefold increase in the lifetime of the Eu ($^5D_0$) level (Table 5). This can be explained by elimination of the non-radiative deactivation pathway through O–H vibrations, as reported previously for many hydrated lanthanide(III) β-diketonates.[5] The improvement in the luminescent properties upon introduction of 4-cpyNO is further substantiated by the determination of the absolute quantum yields (Q^L_{Ln}) for solid samples of the Eu^{III} and Tb^{III} complexes (cf. Table 5). The greatest effect is observed for Eu^{III} compounds, with an approximately tenfold enhancement in Q^L_{Ln}, while the quantum yield of the corresponding Tb^{III} dimer increases only by a factor of 2. This result is in agreement with the evaluated energy gaps between the luminescent levels of Eu^{III} and Tb^{III} ions and the triplet state of 4-cpyNO (vide supra, Table 3).

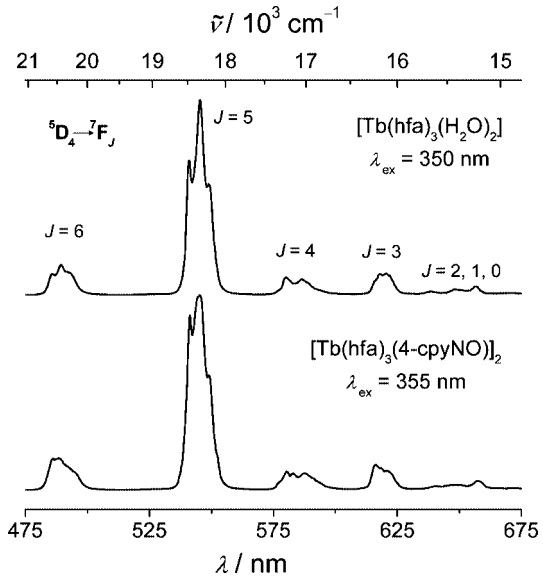

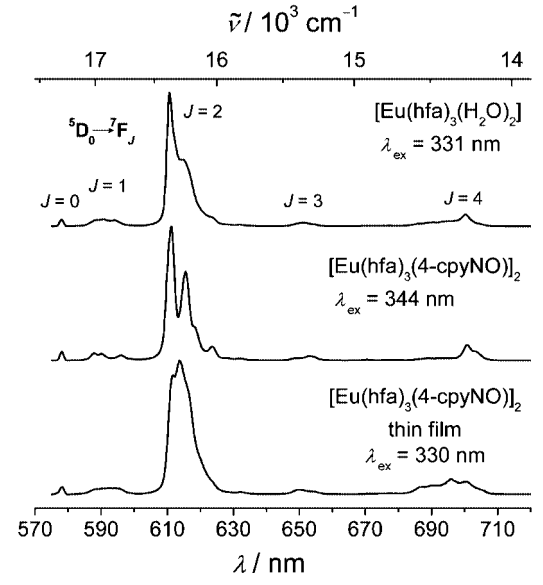

Figure 8. Emission spectra of $[Ln(hfa)_3(H_2O)_2]$ and mixed-ligand $[Ln(hfa)_3(4\text{-cpyNO})]_2$ complexes (Ln = Eu^{III}, Tb^{III}) under ligand excitation at 295 K.

Table 4. Integral intensities of the $^5D_0 \rightarrow {}^7F_J$ and $^5D_4 \rightarrow {}^7F_J$ transitions for the Eu^{III} and Tb^{III} complexes at 295 K relative to the $^5D_0 \rightarrow {}^7F_1$ and $^5D_4 \rightarrow {}^7F_5$ transitions, respectively.

	$\int_{0-0}$	$\int_{0-1}$	$\int_{0-2}$	$\int_{0-3}$	$\int_{0-4}$
$[Eu(hfa)_3(H_2O)_2]$	0.17	1.00	14.30	0.38	1.72
$[Eu(hfa)_3(4\text{-cpyNO})]_2$	0.24	1.00	17.00	0.54	2.16
$[Eu(hfa)_3(4\text{-cpyNO})]_2$, thin film	0.23	1.00	17.95	0.42	2.42
	$\int_{4-6}$	$\int_{4-5}$	$\int_{4-4}$	$\int_{4-3}$	$\int_{4-2,1,0}$
$[Tb(hfa)_3(H_2O)_2]$	0.22	1.00	0.11	0.08	0.04
$[Tb(hfa)_3(4\text{-cpyNO})]_2$	0.23	1.00	0.11	0.08	0.04

For lanthanide(III) complexes, the efficiency of the overall ligand-to-metal energy transfer (η_{sens}) can be estimated from Equation (2),[21] where Q^L_{Ln} is the overall quantum yield upon ligand excitation, η_{et} is the efficiency of the $^3\pi\pi^*$–Ln energy transfer, η_{isc} is the efficiency of the intersystem crossing, Q^{Ln}_{Ln} is the intrinsic quantum yield upon direct excitation of the lanthanide(III) ion, τ_{obs} is the observed lifetime and τ_{rad} is the radiative lifetime (i.e. the lifetime in the absence of any non-radiative process).

As the intensity of the purely magnetic dipole transition ($^5D_0 \rightarrow {}^7F_1$) for europium(III) is independent of the chemical environment around the metal ion, the intrinsic quantum yield may be estimated from Equation (3),[21] where $A_{MD,0}$ = 14.65 s^{-1} is the spontaneous emission probability of the magnetic dipole $^5D_0 \rightarrow {}^7F_1$ transition, n is the refractive index, I_{tot} is the integrated emission of the $^5D_0 \rightarrow {}^7F_J$ (J = 0–4) transitions and I_{MD} is the integrated emission of the $^5D_0 \rightarrow {}^7F_1$ transition.

From the data obtained (Table 5), it can be concluded that the substitution of water molecules by 4-cpyNO leads to a 3.4-fold increase in the intrinsic quantum yield (from

Table 5. Observed and radiative luminescence lifetimes, intrinsic and absolute (±10%) quantum yields, and sensitisation efficiency of $[Ln(hfa)_3(H_2O)_2]$ and $[Ln(hfa)_3(4\text{-cpyNO})]_2$ (Ln = Eu^{III}, Tb^{III}) at 295 K.[a]

Compound	$\tilde{\nu}/\lambda_{em}$ [cm^{-1}/nm]	τ_{obs} [ms]	τ_{rad} [ms]	Q^{Eu}_{Eu} [%]	Q^{L}_{Ln} [%]	η_{sens} [%]
$[Eu(hfa)_3(H_2O)_2]$	16375/610.7	0.22 ± 0.01	1.13	19	2.6	13 ± 2
$[Eu(hfa)_3(4\text{-cpyNO})]_2$	16359/611.3	0.61 ± 0.01	0.95	65	25.7	40 ± 6
$[Eu(hfa)_3(4\text{-cpyNO})]_2$, thin film	16359/611.3	0.74 ± 0.03	0.90	82	[b]	31 ± 5[c]
$[Tb(hfa)_3(H_2O)_2]$	18349/544.0	0.53 ± 0.04[d]	[b]	[b]	26.7	[b]
$[Tb(hfa)_3(4\text{-cpyNO})]_2$	18349/544.0	0.44 ± 0.05[d]	[b]	[b]	49.3	[b]

[a] τ_{rad}, Q^{Eu}_{Eu} and η_{sens} were calculated under the assumption that refractive indices are the same for thin film and solid samples, and equal to 1.5109 for $[Eu(hfa)_3(4\text{-cpyNO})]_2$ and 1.51 for $[Eu(hfa)_3(H_2O)_2]$. [b] Not determined. [c] Calculated under the assumption that the overall quantum yield is the same as for the solid sample. [d] τ_{obs} is almost the same upon excitation of either ligand or terbium(III) levels.

$$Q^{L}_{Ln} = \eta_{sens} Q^{Ln}_{Ln} = \eta_{et}\eta_{isc} Q^{Ln}_{Ln} = \eta_{et}\eta_{isc} \cdot \frac{\tau_{obs}}{\tau_{rad}}, \quad (2)$$

$$Q^{Eu}_{Eu} = \tau_{obs} A_{MD,0} n^3 \cdot \frac{I_{tot}}{I_{MD}}, \quad (3)$$

19 to 65%) and to a 3.1-fold enhancement (from 13 to 40%) of η_{sens}, respectively. Thus, the ancillary ligand significantly contributes to the overall sensitisation process of the Eu^{III} complexes and, additionally, removes part of the quenching processes. In the case of the Tb^{III} compounds, the lifetimes measured upon excitation of either the ligand or the Tb^{III} ion are almost the same, within experimental errors, the lifetime of the mixed-ligand $[Tb(hfa)_3(4\text{-cpyNO})]_2$ dimer being only slightly shorter than that of the parent $[Tb(hfa)_3(H_2O)_2]$ (Table 5). This can be traced back to a larger energy gap displayed by this ion, which means that the contribution of the water molecules to the non-radiative de-excitation processes is smaller than for europium(III).[20,22] Additionally, a lower energy of the triplet state in the mixed-ligand complex relative to the luminescent Tb^{III} levels (Table 3) allows a more efficient back-transfer process, which means that the improvement found in the quantum yield upon binding the ancillary ligand for this ion is entirely due to better sensitisation efficiency.

In the excitation spectrum of a thin film of $[Eu(hfa)_3(4\text{-cpyNO})]_2$, the shoulder feature at 360 nm (27778 cm^{-1}) disappears when compared with the bulk sample (cf. Figure 6), thereby displaying a better correspondence with the reflectance/absorption spectra. This can be explained by the very strong absorption up to 330 nm in the bulk $[Eu(hfa)_3(4\text{-cpyNO})]_2$, which leads to absorption of the incident light only by the near-surface region of the sample while excitation higher than 330 nm will be absorbed throughout the bulk sample. The photoluminescence spectra of the thin film are very similar to those of the bulk sample (cf. Figure 8). On the other hand, the integral intensity of the hypersensitive $^5D_0 \rightarrow {}^7F_{2,4}$ transitions (cf. Table 4) is larger for the thin film than for the bulk sample and this is also the case for the observed luminescence lifetimes and evaluated intrinsic quantum yields (cf. Table 5). These results can be attributed to the higher order of packing of the $[Eu(hfa)_3(4\text{-cpyNO})]_2$ dimers in the thin film than in the bulk solid sample, which, in turn, results in a decrease in the energy transfer rate constants and in a longer luminescence lifetime.

The effect of the mixed-ligand complex formation with 4-cyanopyridine *N*-oxide on the luminescent properties has also been studied for the Sm^{III}, Dy^{III} and Tm^{III} hexafluoroacetylacetonates. The excitation of both $[Ln(hfa)_3(H_2O)_2]$ and $[Ln(hfa)_3(4\text{-cpyNO})]_2$ (Ln = Sm^{III}, Dy^{III}, Tm^{III}) into the ligand-centred band (337 nm) results in characteristic line-like emissions of the corresponding lanthanide ion (Figure 9 and Figures S2 and S3 in the Supporting Information). The luminescence spectra of $[Ln(hfa)_3(H_2O)_2]$ and $[Ln(hfa)_3(4\text{-cpyNO})]_2$ for a given lanthanide ion display the same features. It should be noted that no emission from the lowest triplet state of the ligands has been observed, which reflects the existence of a $^3\pi\pi^*$–Ln energy transfer. The samarium(III) and dysprosium(III) complexes exhibit pink and yellow emission due to $^4G_{5/2} \rightarrow {}^6H_J$ (J = 5/2, 7/2, 9/2, 11/2) and $^4F_{9/2} \rightarrow {}^6H_J$ (J = 13/2, 11/2, 9/2) transitions, with the most intense bands centred at 647 ($^4G_{5/2} \rightarrow {}^6H_{9/2}$) and 573 nm ($^4F_{9/2} \rightarrow {}^6H_{11/2}$), respectively. The excitation spectra of $[Ln(hfa)_3(H_2O)_2]$ and $[Ln(hfa)_3(4\text{-cpyNO})]_2$ (Ln = Sm^{III} and Dy^{III}) are very similar in shape (Figure S1 in the Supporting Information) and present two broad bands around 270 (37000) and 350 nm (28500 cm^{-1}), respectively, which match the corresponding features in the reflectance spectra (see Figure S4 in the Supporting Information). This confirms that the energy transfer takes place from the organic ligands to the lanthanide ions. The excitation spectra also display features corresponding to the metal-centred transitions at around 363 ($^4D_{3/2} \leftarrow {}^6H_{5/2}$), 377 ($^6P_{7/2} \leftarrow {}^6H_{5/2}$), 405 ($^6P_{3/2} \leftarrow {}^6H_{5/2}$) and 420 nm ($^6P_{5/2}$, $^4P_{5/2} \leftarrow {}^6H_{5/2}$) for Sm^{III}, and around 365 ($^4M_{9/2} \leftarrow {}^6H_{15/2}$), 389 ($^4F_{7/2} \leftarrow {}^6H_{15/2}$), 434 ($^4G_{11/2} \leftarrow {}^6H_{15/2}$), 454 ($^4I_{15/2} \leftarrow {}^6H_{15/2}$) and 474 nm ($^4F_{9/2} \leftarrow {}^6H_{15/2}$) for the Dy^{III} derivative. The $[Tm(hfa)_3(H_2O)_2]$ and $[Tm(hfa)_3(4\text{-cpyNO})]_2$ samples were found to be luminescent only at 77 K. Excitation in the ligand absorption band (337 nm) results in blue luminescence with a maximum at 480 nm, which can be assigned to the $^1G_4 \rightarrow {}^3H_6$ transition. The substitution of water molecules in $[Ln(hfa)_3(H_2O)_2]$ (Ln = Sm^{III}, Dy^{III}, Tm^{III}) by 4-cyanopyridine *N*-oxide leads to a decrease of both the luminescence intensity and quantum yields. When compared with the

parent hydrated compounds, the relative quantum yields, $Q_{rel}^{Ln,L}$, of the mixed-ligand Sm^{III} and Dy^{III} complexes are 0.55 ± 0.06 and 0.50 ± 0.05, respectively. The most drastic decrease occurs for the Tm^{III} adduct, leading to a $Q_{rel}^{Ln,L}$ value of 0.19 ± 0.02. This is probably due to multi-phonon deactivation of the excited states for the respective lanthanide ions by the N–O vibrations of 4-cyanopyridine *N*-oxide. The efficacy of this quenching process is inversely proportional to the energy gap between the emitting state and the ground state manifold: the larger the energy gap, the lower the non-radiative rate constant will be as the number of phonons necessary to bridge the gap increases in this case.[22] So, this quenching is more significant for Sm^{III}, Dy^{III} and Tm^{III} than for Eu^{III} or Tb^{III} because the energy gaps between the luminescent state and ground-state manifold are not large for the former (7400 for Sm^{III}, 7850 for Dy^{III} and 5800 cm^{-1} for Tm^{III}) when compared with the values for Eu^{III} or Tb^{III} (12300 and 14800 cm^{-1}, respectively). Although the main vibrations of the N–O bonds in 4-cpyNO are not too energetic (around 1280 cm^{-1}), they contribute substantially to the quenching process: approximately 6, 6, and 4–5 phonons are required to bridge the energy gap of Sm^{III}, Dy^{III} and Tm^{III}, respectively. Moreover, in the mixed-ligand Dy^{III} and Tm^{III} complexes, poor luminescence sensitisation may be caused by poorly matched energy gaps between the triplet state of the ancillary ligand and the luminescent levels of these ions (Table 3).

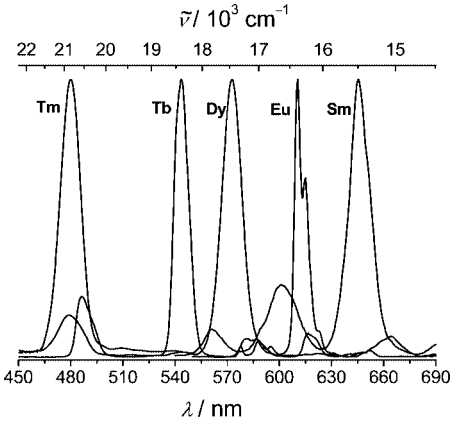

Figure 9. Emission spectra of mixed-ligand dimeric complexes $[Ln(hfa)_3(4\text{-cpyNO})]_2$ (Ln = Tm^{III}, Tb^{III}, Dy^{III}, Eu^{III}, Sm^{III}) under ligand excitation (see also Figure S3).

Conclusions

The reaction of lanthanide hexafluoroacetylacetonates $[Ln(hfa)_3(H_2O)_2]$ (Ln = Sm^{III}–Ho^{III}, and Tm^{III}) with 4-cyanopyridine *N*-oxide in a 1:1 ratio results in the formation of $[Ln(hfa)_3(4\text{-cpyNO})]_2$ dimers in which the two metal ions are separated by about 3.99–4.13 Å. The magnetic studies reveal weak antiferromagnetic exchange interactions between neighbouring metal centres within the dimeric $[Gd(hfa)_3(4\text{-cpyNO})]_2$ units. The substitution of water molecules in the parent hydrated complexes $[Ln(hfa)_3(H_2O)_2]$ by 4-cpyNO has a large effect on the luminescence properties. Such a combination of organic ligands is able to sensitize the metal-centred luminescence of Sm^{III}, Eu^{III}, Tb^{III}, Dy^{III} and Tm^{III} ions that emit pink, red, green, yellow and blue light, respectively, i.e. within the entire spectral visible range. The introduction of the ancillary ligand leads to substantial and varying changes in the luminescence quantum yields. The greatest effect occurs for $[Eu(hfa)_3(4\text{-cpyNO})]_2$, with a tenfold increase in the absolute quantum yield (from 2.6 to 25.7%) with respect to the hydrated complex. On the other hand, a decrease in the quantum yield is observed for Sm^{III}, Dy^{III} and Tm^{III} dimers with respect to the hydrated chelates. The $[Ln(hfa)_3(4\text{-cpyNO})]_2$ dimers are thermally stable up to 190 °C and can be quantitatively sublimed at 200 °C under reduced pressure (10^{-2} Torr), thus opening the way to the production of luminescent thin films, as demonstrated here with Eu^{III}. Both the luminescence lifetime and intrinsic quantum yield of Eu^{III} are higher in thin films than in the solid sample, while the sensitisation efficacy remains approximately the same. In conclusion, high volatility, good thermal stability and efficient luminescent properties make the mixed-ligand $[Ln(hfa)_3(4\text{-cpyNO})]_2$ complexes, especially the Eu^{III} and Tb^{III} derivatives, good candidates for emitting layers in light-emitting diodes.

Experimental Section

Reagents and Physical Methods: The commercially available starting reagents Hhfa (Merck) and 4-cyanopyridine *N*-oxide (Aldrich) were of analytical grade and used as received. Lanthanide nitrate hydrates $Ln(NO_3)_3 \cdot xH_2O$ were obtained by treating the respective lanthanide oxides Ln_2O_3 (99.998%) with concentrated nitric acid, followed by evaporation of the excess acid. For the synthesis of $[Ln(hfa)_3(H_2O)_2]$ (Ln = Sm^{III}–Ho^{III}, and Tm^{III}) the procedure described in ref.[23] was used. Elemental analysis (C, H, N) was performed by the Microanalytical Service of the Centre for Drug Chemistry (Moscow, Russia). The lanthanide content was determined by titrimetric analysis.[24] IR spectra were recorded in Nujol mull or hexachlorobutadiene between KBr plates in the range 4000–400 cm^{-1} using a Perkin–Elmer 1600 FT-IR spectrometer. Thermogravimetric analyses were performed with a Q-1500 thermal analyzer under nitrogen, at a heating rate of 10 °C min^{-1}. Isothermal dynamic sublimation experiments were run with samples (ca. 100 mg) placed into glass test tubes at 20–220 °C and a pressure of 10^{-2} Torr for periods of about 30 min. Weight loss was essentially 100%. The homogeneous sublimate was collected in the cold part of the tube and analysed.

Syntheses: All lanthanide(III) hexafluoroacetylacetonate adducts $[Ln(hfa)_3(4\text{-cpyNO})]_2$ (Ln = Sm^{III}–Ho^{III}, Tm^{III}) were synthesised in a similar way. A typical preparation procedure is as follows: 4-Cyanopyridine *N*-oxide (60 mg, 0.5 mmol) was added to a solution of $[Ln(hfa)_3(H_2O)_2]$ (0.5 mmol) in chloroform (20 mL). The resulting mixture was then stirred at room temperature for 1 h. Further evaporation of the solvent under low pressure yielded a colourless (Gd^{III}, Tb^{III}), pale yellow (Sm^{III}, Eu^{III}, Ho^{III} and Dy^{III}) or pale aquamarine (Tm^{III}) polycrystalline precipitate, which was filtered off and dried in air. Yield: 80–90%.

$C_{42}H_{14}F_{36}N_4O_{14}Sm_2$ (1783.3): calcd. C 28.25, H 0.78, N 3.14, Sm 16.8; found C 28.0, H 0.8, N 3.2, Sm 16.7. IR: $\tilde{\nu}$ = 3140 m, 3106 m,

3076 m, 2262 w, 1650 vs, 1612 m, 1560 s, 1534 s, 1490 s, 1394 w, 1350 m, 1324 m, 1258 br. s, 1210 br. s, 1144 br. s, 1098 s, 950 w, 852 s, 802 s, 772 w, 740 s, 724 s, 660 s, 586 s, 558 m, 528 w, 488 w, 456 br. w cm^{-1}.

$C_{42}H_{14}Eu_2F_{36}N_4O_{14}$ (1786.5): calcd. C 28.19, H 0.78, Eu 17.0, N 3.13; found C 28.43, H 0.89, Eu 16.9, N 3.38. IR: $\tilde{\nu}$ = 3132 m, 3102 m, 3078 m, 2258 w, 1660 vs, 1650 s, 1612 m, 1562 s, 1538 s, 1498 s, 1464 s, 1448 m, 1440 m, 1394 w, 1350 m, 1324 m, 1254 br. s, 1218 br. s, 1148 br. s, 1108 s, 1100 s, 950 w, 860 m, 850 s, 806 s, 770 w, 742 m, 734 m, 660 s, 588 s, 560 w, 554 w, 528 w, 486 w, 474 w, 456 w cm^{-1}.

$C_{42}H_{14}F_{36}Gd_2N_4O_{14}$ (1797.0): calcd. C 28.03, H 0.78, Gd 17.5, N 3.11; found C 27.89, H 0.79, Gd 17.3, N 3.07. IR: $\tilde{\nu}$ = 3132 m, 3102 m, 3080 m, 2260 w, 1660 vs, 1650 s, 1612 m, 1562 s, 1538 s, 1500 s, 1446 s, 1446 m, 1394 w, 1350 m, 1324 m, 1268 s, 1254 br. s, 1146 br. s, 1216 br. s, 1108 s, 1100 s, 952 w, 862 m, 850 s, 804 s, 770 w, 742 m, 734 m, 662 s, 588 s, 560 w, 554 w, 528 w, 488 w, 476 w, 456 w cm^{-1}.

$C_{42}H_{14}F_{36}N_4O_{14}Tb_2$ (1800.4): calcd. C 27.97, H 0.78, N 3.11, Tb 17.6; found C 27.71, H 0.74, N 3.05, Tb 17.5. IR: $\tilde{\nu}$ = 3134 m, 3102 m, 3080 m, 2262 w, 1658 vs, 1650 s, 1612 m, 1562 s, 1358 s, 1502 s, 1464 s, 1442 m, 1396 w, 1352 m, 1268 s, 1254 br. s, 1216 br. s, 1146 br. s, 1100 s, 974 w, 952 w, 862 m, 850 s, 804 s, 770 w, 742 m, 734 m, 662 s, 588 s, 562 w, 528 w, 490 w, 476 w, 456 w cm^{-1}.

$C_{42}H_{14}Dy_2F_{36}N_4O_{14}$ (1807.5): calcd. C 27.86, H 0.77, Dy 18.0, N 3.09; found C 28.50, H 0.81, Dy 17.9, N 3.17. IR: $\tilde{\nu}$ = 3142 m, 3106 m, 3080 m, 2256 w, 1652 br. s, 1616 m, 1564 s, 1540 s, 1506 s, 1492 s, 1466 s, 1442 m, 1394 w, 1354 m, 1256 br. s, 1212 br. s, 1146 br. s, 1100 s, 1038 m, 980 w, 952 w, 852 s, 806 s, 772 w, 734 m, 722 m, 660 s, 588 s, 564 w, 528 w, 494 w, 480 w, 458 w cm^{-1}.

$C_{42}H_{14}F_{36}Ho_2N_4O_{14}$ (1812.4): calcd. C 27.78, H 0.77, Ho 18.2, N 3.09; found C 27.95, H 0.82, Ho 18.2, N 3.12. IR: $\tilde{\nu}$ = 3140 m, 3104 m, 3080 m, 2260 w, 1664 s, 1652 s, 1612 m, 1564 s, 1538 s, 1506 s, 1490 s, 1482 s, 1448 m, 1354 m, 1338 m, 1265 s, 1250 br. s, 1216 br. s, 1146 br. s, 1102 s, 952 w, 864 m, 850 s, 804 s, 773 w, 742 m, 734 m, 662 s, 588 s, 560 w, 527 w, 496 w, 480 w, 454 w cm^{-1}.

$C_{42}H_{14}F_{36}N_4O_{14}Tm_2$ (1820.4): calcd. C 27.66, H 0.77, Tm 18.6, N 3.07; found C 27.68, H 0.79, Tm 18.6, N 3.12. IR: $\tilde{\nu}$ = 3138 m, 3104 m, 3082 m, 2262 w, 1664 s, 1652 s, 1612 m, 1564 s, 1538 s, 1506 s, 1490 s, 1482 s, 1466 s, 1448 m, 1354 m, 1338 m, 1270 s, 1254 br. s, 1216 br. s, 1146 br. s, 1102 s, 952 w, 864 m, 852 s, 804 s, 770 w, 742 m, 734 m, 662 s, 588 s, 560 w, 528 w, 496 w, 482 w, 454 w cm^{-1}.

The monomeric complex $[Gd(NO_3)_3(4\text{-cpyNO})]$ was prepared in ethanol by a similar procedure as described above for $[Ln(hfa)_3(4\text{-cpyNO})]_2$. Yield: 90%. $C_6H_4GdN_5O_{10}$ (463.38): calcd. Gd 33.9; found Gd 33.9. IR: $\tilde{\nu}$ = 3116 m, 3084 m, 3062 m, 3032 m, 2246 m, 1648 m, 1620 m, 1488 m, 1456 m, 1438 m, 1378 m, 1324 s, 1238 s, 1222 m, 1180 m, 1110 w, 1044 w, 1032 m, 974 w, 864 m, 858 m, 818 w, 734 m, 634 br. w, 584 w, 560 m, 478 w, 462 w, 436 w cm^{-1}.

Data Collection and Structural Refinement: Single crystals suitable for X-ray analysis were obtained by recrystallisation of the crude products from chloroform. Diffraction data were collected with an image-plate diffractometer (Stoe IPDS) for the Tb^{III} complex and with a four-circle CCD diffractometer (Stoe STADI4) for the Ho^{III} derivative, using graphite-monochromated Mo-K_α radiation (λ = 0.71073 Å). The structures were solved by direct methods (SHELXS-97)[25] and refined anisotropically for all non-hydrogen atoms by employing full-matrix least squares on F^2 (SHELXL-97).[26] The hydrogen atoms were included in the calculated positions and refined in a riding mode. Crystallographic data and some details of data collection and structure refinement are listed in Table 6. CCDC-612981 and -612982 contain the supplementary crystallographic data for this paper. These data can be obtained free of charge from The Cambridge Crystallographic Data Centre via www.ccdc.cam.ac.uk/data_request/cif.

Diffuse Reflectivity Spectra: UV/Vis reflectance spectra for solid samples of Sm^{III}, Dy^{III} and Tm^{III} complexes (Figure S4 in the Supporting Information) were recorded with a Lambda 35 spectrophotometer (Perkin–Elmer). The absorption spectra (absorption coefficient α over scattering coefficient σ as a function of wavelength) were extracted from the diffuse reflectance spectra of the "infinitely thick" powder samples (R_∞), using the Kubelka–Munk function, $\frac{\alpha}{\sigma} = \frac{(1-R_\infty)^2}{2R_\infty}$. Plots of the corresponding Kubelka–Munk functions are shown in Figure S5.

Table 6. Crystallographic data and some details of data collection and structure refinement for $[Ln(hfa)_3(4\text{-cpyNO})]_2$ complexes (Ln = Tb^{III}, Ho^{III}).

	$[Tb(hfa)_3(4\text{-cpyNO})]_2$	$[Ho(hfa)_3(4\text{-cpyNO})]_2$
Empirical formula	$C_{42}H_{14}F_{36}N_4O_{14}Tb_2$	$C_{42}H_{14}F_{36}N_4O_{14}Ho_2$
Formula mass	1800.42	1812.44
Crystal system	monoclinic	monoclinic
Space group	$P2_1/c$ (no. 14)	$P2_1/c$ (no. 14)
a [Å]	18.918(4)	18.636(5)
b [Å]	18.552(4)	18.110(5)
c [Å]	17.420(3)	17.099(5)
β [°]	92.90(3)	93.95(3)
V [Å^3]	6106(2)	5757(3)
Z	4	4
$\rho_{calcd.}$ [g cm^{-3}]	1.959	2.091
T [K]	293(2)	160(2)
Crystal size [mm]	0.25 × 0.20 × 0.16	0.60 × 0.40 × 0.25
Absorption coefficient μ [cm^{-1}]	24.68	29.10
Reflections collected	41843	9740
Data/parameters	12937/883	9740/883
R_1 [$I > 2\sigma(I)$]	0.0356	0.0474
ωR_2 (all data)	0.0881	0.1004
Goodness-of-fit on F^2	0.842	1.087

Luminescence Measurements: Solid samples were ground into fine powders prior to the luminescence measurements. Excitation and photoluminescence spectra of Sm^{III} and Dy^{III} adducts were recorded at 295 K with a Perkin–Elmer LS-55 luminescence spectrometer (λ_{ex} = 337 nm, xenon lamp). Luminescence spectra of Gd^{III} and Tm^{III} complexes were measured at 77 K with a multichannel spectrometer S2000 (Ocean Optics) utilizing a nitrogen laser LGI-21 (λ_{ex} = 337 nm) as an excitation source. The luminescence data (excitation spectra, lifetimes and absolute quantum yields) of Eu^{III} and Tb^{III} derivatives were recorded at 295 K with a Fluorolog FL3-22 spectrofluorimeter from Horiba–Jobin–Yvon–Spex; to prevent saturation of the signal in photon-counting mode, the emission bandpass was set to 1 nm. Excitation spectra were measured by monitoring the characteristic $^4G_{5/2}\rightarrow{}^6H_{9/2}$, $^5D_0\rightarrow{}^7F_2$, $^5D_4\rightarrow{}^7F_5$ and $^4F_{9/2}\rightarrow{}^6H_{11/2}$ transitions for Sm^{III}, Eu^{III}, Tb^{III} and Dy^{III}, respectively. Luminescence lifetimes (τ_{obs}) of the Eu^{III} compounds were determined by excitation of the $^5D_2$ level (466 nm, 21459 cm^{-1}) and monitoring the $^5D_0\rightarrow{}^7F_2$ transition, while those of the Tb^{III} complexes were measured by excitation of either the Tb^{III} ion or the ligand and monitoring the $^5D_4\rightarrow{}^7F_5$ transition. Lifetimes are the averages of at least three independent measurements. All luminescence decays proved to be perfect single exponential functions. All excitation and luminescence spectra were corrected by the instrumental functions. Electronic transitions were assigned by comparing the measured spectra with those reported by Elyashevich[27] and in other previous studies.[28] Luminescence quantum yields of $[Ln(hfa)_3(H_2O)_2]$ and $[Ln(hfa)_3(4\text{-cpyNO})]_2$ (Ln = Eu^{III}, Tb^{III}) were determined for solid samples by excitation into the ligand absorption band, according to the absolute method of Wrighton.[29] Each sample was measured several times under slightly different experimental conditions. Relative quantum yields, $Q_{rel}^{Ln,L}$, of Sm^{III}, Dy^{III} and Tm^{III} chelates $[Ln(hfa)_3(4\text{-cpyNO})]_2$ were calculated relative to the respective $[Ln(hfa)_3(H_2O)_2]$ complexes (at the same excitation wavelength and experimental geometry), using Equation (4), where Q is the quantum yield, R is the amount of reflected excitation radiation, ϕ is the integrated area of the corrected luminescence spectra and the indexes x and r correspond to $[Ln(hfa)_3(4\text{-cpyNO})]_2$ and $[Ln(hfa)_3(H_2O)_2]$, respectively. For comparison reasons, Q_r was set to 1. The estimated error for the luminescence quantum yields is ±10%.

$$Q_{rel}^{Ln,L} = \frac{Q_x}{Q_r} = \left(\frac{1-R_r}{1-R_x}\right)\left(\frac{\phi_x}{\phi_r}\right) \quad (4)$$

Refractive Index and Thickness of Thin Films: Thin films of $[Eu(hfa)_3(4\text{-cpyNO})]_2$ were deposited on quartz substrates by the thermal evaporation method in a vacuum chamber ($P \approx 10^{-6}$ Torr, Leybold Heraeus). The refractive index (n) and layer thickness (d) were measured with a Filmetric F20 Thin Film Analyzer. The results are averages of at least three measurements. $[Eu(hfa)_3(4\text{-cpyNO})]_2$ (thin film): $n = 1.511 \pm 0.002$, $d = 414 \pm 1$ nm.

Magnetic Measurements: Magnetic susceptibility data (2–300 K) for polycrystalline samples of $[Ln(hfa)_3(4\text{-cpyNO})]_2$ (Ln = Gd^{III}, Tb^{III}) were collected with a SQUID magnetometer using a Quantum Design MPMS instrument with applied DC magnetic fields of 200 and 1000 Oe, respectively. The experimental data were corrected for the sample holder contribution and for diamagnetism of the constituent atoms estimated from Pascal's increments.[30]

Supporting Information (see footnote on the first page of this article): Reflection, excitation and photoluminescence spectra.

Acknowledgments

We are grateful to Prof. Ritta Szymczak and Dr. Marek Baran (Institute of Physics, Polish Academy of Sciences) for the magnetic measurements, Mr. Andrei A. Vaschenko (Lebedev Physical Institute of Russian Academy of Sciences) for his assistance in obtaining thin-film samples, and the Russian Foundation for Basic Research (RFBR, grants 05-03-33090, 04-02-17040) for financial support.

[1] J. Kido, Y. Okamoto, *Chem. Rev.* **2002**, *102*, 2357–2368 and references cited therein.
[2] S. Faulkner, S. J. A. Pope, B. P. Burton-Pye, *Appl. Spectrosc. Rev.* **2005**, *40*, 1–31 and references cited therein.
[3] V. W. W. Yam, K. K. W. Lo, *Coord. Chem. Rev.* **1999**, *184*, 157–240 and references cited therein.
[4] J.-C. G. Bünzli, C. Piguet, *Chem. Soc. Rev.* **2005**, *34*, 1048–1077.
[5] K. Binnemans, in *Handbook on the Physics and Chemistry of Rare Earths* (Eds.: K. A. Gschneidner Jr, J.-C. G. Bünzli, V. K. Pecharsky), Elsevier, Amsterdam, **2005**, vol. 35, chapter 225.
[6] J.-C. G. Bünzli, in *Lanthanide Probes in Life, Chemical and Earth Sciences. Theory and Practice* (Eds.: J.-C. G. Bünzli, G. R. Choppin), Elsevier, Amsterdam, Oxford, New York, Tokyo, **1989**, chapter 7.
[7] See for example: P. Lenaerts, A. Storms, J. Mullens, J. D′Haen, C. Görller-Walrand, K. Binnemans, K. Driesen, *Chem. Mater.* **2005**, *17*, 5194–5201; S. W. Magennis, A. J. Ferguson, T. Bryden, T. S. Jones, A. Beeby, I. D. W. Samuel, *Synth. Met.* **2003**, *138*, 463–469; R. Reisfeld, T. Saraidarov, M. Pietraszkiewicz, S. Lis, *Chem. Phys. Lett.* **2001**, *349*, 266–270; H. Suzuki, Y. Hattori, T. Iizuka, K. Yuzawa, N. Matsumoto, *Thin Solid Films* **2003**, *438–439*, 288–293.
[8] K. Nakanishi, *IR Spectroscopy and Structure of Organic Compounds*, Mir, Moscow, **1965** (in Russian).
[9] E. L. Muetterties, L. J. Guggenberger, *J. Am. Chem. Soc.* **1974**, *96*, 1748–1756.
[10] M. G. B. Drew, *Coord. Chem. Rev.* **1977**, *24*, 179–275.
[11] V. A. Petrov, W. J. Marshall, V. V. Grushin, *Chem. Commun.* **2002**, 520–521.
[12] J. P. Gallivan, D. A. Dougherty, *Org. Lett.* **1999**, *1*, 103–105.
[13] M. Ryazanov, S. Troyanov, M. Baran, R. Szymczak, N. Kuzmina, *Polyhedron* **2004**, *23*, 879–883.
[14] I. P. Malkerova, A. S. Alikhanyan, S. V. Eliseeva, N. P. Kuzmina, *Russ. J. Inorg. Chem.*, in press.
[15] S. I. Weissman, *J. Chem. Phys.* **1942**, *10*, 214–217.
[16] N. Sabbatini, M. Guardigli, J.-M. Lehn, *Coord. Chem. Rev.* **1993**, *123*, 201–228.
[17] See for example: G. F. de Sá, O. L. Malta, C. D. Donega, A. M. Simas, R. L. Longa, P. A. Santa-Cruz, E. F. da Silva, *Coord. Chem. Rev.* **2000**, *196*, 165–195; F. R. Conçalves e Silva, O. L. Malta, C. Reinhard, H. U. Güdel, C. Piguet, J. E. Moser, J.-C. G. Bünzli, *J. Phys. Chem. A* **2002**, *106*, 1670–1677; F. R. Conçalves e Silva, R. L. Longo, O. L. Malta, C. Piguet, J.-C. G. Bünzli, *Phys. Chem. Chem. Phys.* **2000**, *2*, 5400–5403.
[18] See for example: M. Latva, H. Takalo, V. M. Mukkala, C. Matachescu, J.-C. Rodriguez-Ubis, J. Kankare, *J. Lumin.* **1997**, *75*, 149–169; F. Gutierrez, C. Tedeschi, L. Maron, J. P. Daudey, R. Poteau, J. Azema, P. Tisnes, C. Picard, *Dalton Trans.* **2004**, 1334–1347; H. J. Kim, J. E. Lee, Y. S. Kim, N. G. Park, *Opt. Mater.* **2002**, *21*, 181–186.
[19] S. Petoud, J.-C. G. Bünzli, T. Glanzman, C. Piguet, Q. Xiang, R. P. Thummel, *J. Lumin.* **1999**, *82*, 69–79.
[20] J.-C. G. Bünzli, in *Spectroscopic Properties of Rare-Earths in Optical Materials* (Eds.: G. Liu, B. Jacquier), Springer-Verlag, Berlin, **2005**, chapter 11.
[21] A.-S. Chauvin, F. Gumy, D. Imbert, J.-C. G. Bünzli, *Spectrosc. Lett.* **2004**, *37*, 517–532.

[22] A. Beeby, I. M. Clarkson, R. S. Dickins, S. Faulkner, D. Parker, L. Royle, A. S. de Sousa, J. A. G. Williams, M. Woods, *J. Chem. Soc., Perkin Trans. 2* **1999**, 493–503.
[23] M. F. Richardson, W. F. Wagner, D. E. Dands, *J. Inorg. Nucl. Chem.* **1968**, *30*, 1275–1289.
[24] R. Prshibil, *Complexones in Chemical Analysis*, Mir, Moscow, **1955** (in Russian).
[25] G. M. Sheldrick, *SHELXS 97, Program for the Solution of Crystal Structures*, University of Göttingen, Germany, **1997**.
[26] G. M. Sheldrick, *SHELXL 97, Program for the Refinement of Crystal Structures*, University of Göttingen, Germany, **1997**.
[27] M. A. Elyashevich, *Spectra of Rare-Earth Elements*, Gosteht-eoretizdat, Moscow, **1953** (in Russian).
[28] See for example: W. T. Carnall, P. R. Fields, K. Rajnak, *J. Chem. Phys.* **1968**, *49*, 4424–4442; W. T. Carnall, P. R. Fields, K. Rajnak, *J. Chem. Phys.* **1968**, *49*, 4443–4446; W. T. Carnall, P. R. Fields, K. Rajnak, *J. Chem. Phys.* **1968**, *49*, 4447–4449; W. T. Carnall, P. R. Fields, K. Rajnak, *J. Chem. Phys.* **1968**, *49*, 4450–4455.
[29] M. S. Wrighton, D. S. Ginley, D. L. Morse, *J. Phys. Chem.* **1974**, *78*, 2229–2233; N. C. Greenham, I. D. W. Samule, G. R. Hayes, R. T. Philips, Y. A. R. R. Kessener, S. C. Moratti, A. B. Holmes, R. H. Friend, *Chem. Phys. Lett.* **1995**, *241*, 89–96; J. C. de Mello, H. F. Wittmann, R. H. Friend, *Adv. Mater.* **1997**, *9*, 230–232.
[30] R. L. Carlin, *Magnetochemistry*, Springer-Verlag, Berlin, **1986**.
Received: July 18, 2006
Published Online: October 18, 2006

